applied sciences

MDPI

Article

Experimental Study on the Effect of Pile-End Soil on the Pile Load Transfer Law

Hangyu Zhang and Hailong Ma *

School of Civil Engineering and Architecture, Zhejiang Sci-Tech University, Hangzhou 310018, China; zhywymail@126.com

* Correspondence: mahailonglg@126.com; Tel.: +86-138-5803-5810

Abstract: This paper compares and analyzes the difference in the skin friction between pile-end soilless compressive pile and conventional compressive pile at various stages during loading by the in situ test method. The influence of pile-end soil on the load transfer law of compressive piles in clay-dominated stratified foundations is further investigated. The results show that the overall load–displacement curves of the pile-end soilless compressive pile and the conventional compressive pile both present a slow decline followed by a steep drop. The length of the linear section on the load–displacement curve of the pile-end soilless compressive pile is less than that of the linear stage of the conventional compressive pile. Under the vertical load, the distribution laws and distribution forms of the skin friction ratio of the pile sections of the two piles are more consistent. The pile-end soil of the conventional compressive pile restricts the skin friction of the pile's middle-lower and lower pile segments when compared to the pile-end soilless compressive pile. This restriction manifests itself as a reduction in pile skin friction, and the weakening effect decreases from bottom to top.

Keywords: compression pile; skin friction; load transfer law; weakening effect; in situ test

Citation: Zhang, H.; Ma, H. Experimental Study on the Effect of Pile-End Soil on the Pile Load Transfer Law. *Appl. Sci.* **2022**, *12*, 6347. https://doi.org/10.3390/app12136347

Academic Editor: Chin Leo

Received: 1 June 2022
Accepted: 20 June 2022
Published: 22 June 2022

1. Introduction

The working principle of pile foundations is that the pile foundation transfers the upper load to the soil around the pile and the soil at the bottom of the pile through contact between the side and bottom of the pile and soil, thus ensuring that the building meets the requirements of foundation stability and the allowable amount of deformation. Therefore, pile–soil interaction [1,2] has become a problem that must be considered in the design of pile foundations. The pile transfers part of the load to the surrounding soil through the frictional shearing action between the pile side and the soil, and the rest of the load is transferred to the pile-end soil through the pile body. Pile section properties [3–5], the pile–soil contact surface [6–8], and pile–soil shear mode [9–11] all affect the interaction between the pile and the surrounding soil.

The single pile bearing capacity calculation of the existing pile foundation is to simply add the pile-end resistance and the skin friction; the default pile-end resistance and pile-side friction resistance do not affect each other. However, a large number of existing research practices show that the pile-end soil affects the exertion of the skin friction, and the measured skin friction of a single pile varies with the strength of the pile-end soil or the pile-bearing stratum. Some studies [12–15] have shown that there is an interaction between skin friction and pile-end resistance; it is mainly manifested in the local strengthening effect of the skin friction at the pile-end. The effect of this strengthening effect is related to the strength of the pile-end soil. The greater the strength of the soil at the pile-end, the more obvious the strengthening effect. Additionally, the mechanism of the strengthening effect of skin friction is explained through Meyerhof's [16] failure mode of pile foundation. Zhang et al. [17] affirmed that the increase of soil strength at the pile-end has a strengthening effect on the skin friction through the measured skin friction

of the static load test of super-long piles and used the Mohr–Coulomb theory to analyze the effect of pile-end soil strength on skin friction. By quantifying the test results of the model test, Liu et al. [18] found that there is a relationship between the frictional shear strength of the pile side and the strength of the pile-end soil. Some studies pointed out that there is a weakening effect of the skin friction at the pile-end. Dong [19] and Xiong [20] pointed out that there is a weakening effect of the skin friction at the pile-end when the soil strength at the pile-end is low through the static load test of the grouted pile. The lower the strength of the soil at the end of the pile, the more obvious the weakening effect. Through numerical analysis, Ju et al. [21] found that when the water content of the sediment at the pile-end is large, excess pore water pressure will appear on the pile–soil contact surface near the pile-end, thereby reducing skin friction. Skin friction at the pile-end shows a weakening phenomenon.

The existing research on the different performances of skin friction at the pile-end is mainly manifested as the strengthening effect and the weakening effect. The studies are based on the presence of pile-end soils, and there are few quantitative studies of the effect of the presence or absence of pile-end soil on the skin friction of pile. This test compares the load transfer laws of two pile types, pile-end soilless compressive pile and conventional compressive pile, in a layered foundation with mainly clay soil. Our aim was to study the load transfer mechanism under vertical load and the difference in the performance of the skin friction traits to analyze and discuss the quantitative effect of the presence of pile-end soil on skin friction.

2. Overview of In Situ Test

2.1. Geological Conditions of the Test Site

The experimental site is located in Changshu City, Suzhou City, Jiangsu Province. The stratum from top to bottom is miscellaneous fill, silty clay, muddy–silty clay, clay, and silty clay. Of which the miscellaneous fill was removed before the start of the test. The soil layer parameters are shown in Table 1.

Table 1. Parameters of each soil layer at the test site.

Soil Layer Number	Soil Layer	Soil Thickness of the Pile-End Soilless Compressive Pile h/m	Soil Thickness of the Conventional Compressive Pile h/m	Ultimate Standard Value of Shaft Resistance q_{si}/kPa
1	Miscellaneous fill	-	-	-
2	Silty clay	1.0	0.9	25
3	Muddy silty clay	2.2	1.9	18
4	Clay	2.2	2.4	65
5	Silty clay	1.0	1.4	55

2.2. Test Pile Preparation and Loading Scheme

To comparatively study the effect of pile-end soil on the skin friction of the pile, two test piles were used: a pile-end soilless compressive pile, and a conventional compressive pile. The depth of the two piles into the ground varied slightly due to the thickness of the stratum (Table 1). The length of the pile was controlled according to entering the bearing layer for clay at 0.6 m. The length of the pile-end soilless compressive pile was 3.8 m, and the length of the conventional compressive pile was 3.4 m. In this test, a steel pipe was used to develop the test pile. The elastic modulus of the pile was 206 GPa, the diameter of the pile was 108 mm, and the wall thickness of the pile was 4 mm.

In order to obtain the strain at different depths of the pile section under load, the steel pipe was divided into four 0.8 m sections of steel pipe and one 1.4 m section of steel

pipe. After the strain gauge was attached to the inner side of the test pile, the steel pipe was welded. The strain gauges were BFH-120-3AA metal strain gauges, the size of the sensitive grid was 3 × 2 mm (length × width), the nominal resistance was 120 Ω, the sensitivity coefficient was 2.08 ± 1%, and the accuracy grade was A. Epoxy glue and silica gel were used on the surface of the strain gauge to prevent the strain gauge from becoming damp when exposed to water in the ground. The strain gauge arrangement is shown in Figure 1. The data acquisition of pile strain gauges was connected and collected by the DH3820 high-speed static strain data acquisition instrument. This high-speed static strain data acquisition instrument had a sampling frequency of 100 Hz, which can accurately acquire and record the slow change signal in the test to ensure the accuracy of the test acquisition data.

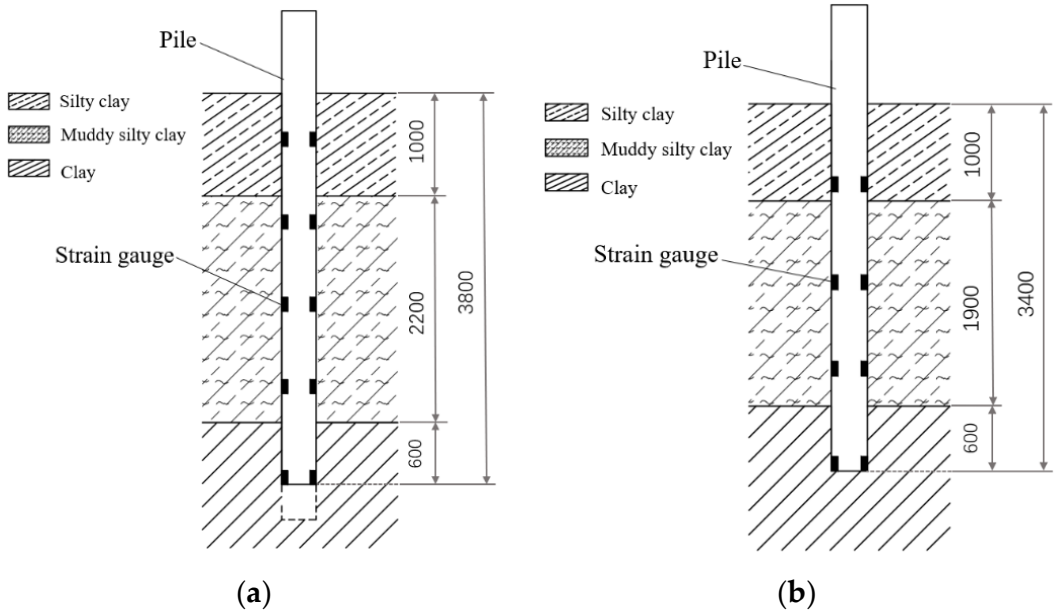

Figure 1. Schematic diagram of the position of the strain gauge in the test pile: (**a**) the pile-end soilless compressive pile and (**b**) the conventional compressive pile.

The pile tip of the pile-end soilless compressive pile was separated from the pile body, as shown in Figure 2. After the pile-end soilless compressive pile was pressed to the design position, it was then pulled up by 50 mm, and the pile tip was separated from the pile body to form a pile-end soilless compressive pile. The static load test was carried out after 28 d of pile construction, and the test was carried out by the slow maintenance load method [22]. Load–displacement curves and displacement–time logarithm curves were obtained. The site was loaded, as shown in Figure 3. Simultaneous recordings of the strain gauge readings were carried out during loading.

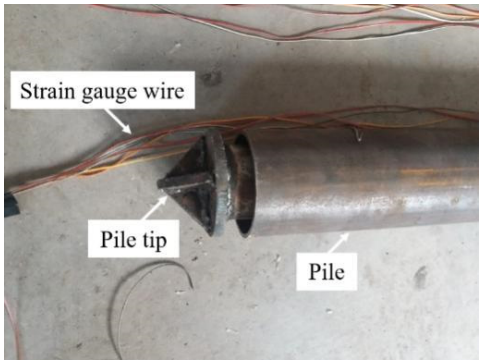

Figure 2. Schematic diagram of the pile-end soilless compressive pile.

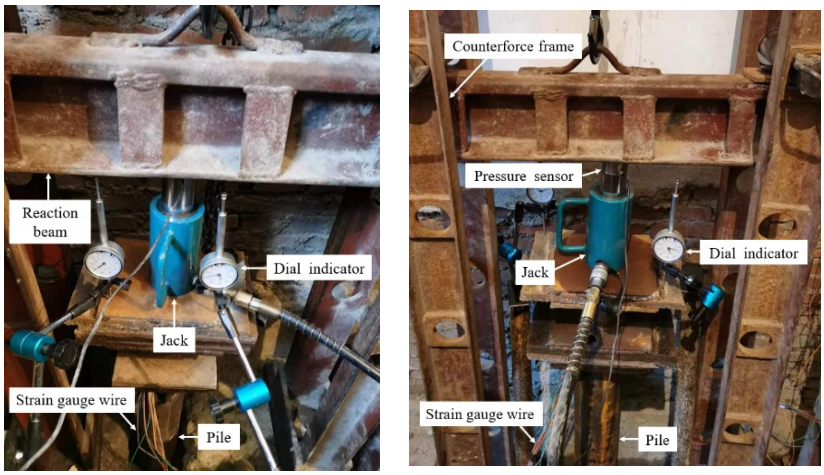

(**a**) (**b**)

Figure 3. Schematic diagram of test pile loading: (**a**) the pile-end soilless compressive pile and (**b**) the conventional compressive pile.

3. Analysis of Test Results

3.1. Load Displacement Relationship

According to the test results, the load–displacement curves (Q-s curve) of the pile-end soilless compressive pile and the conventional compressive pile are plotted as shown in Figure 4.

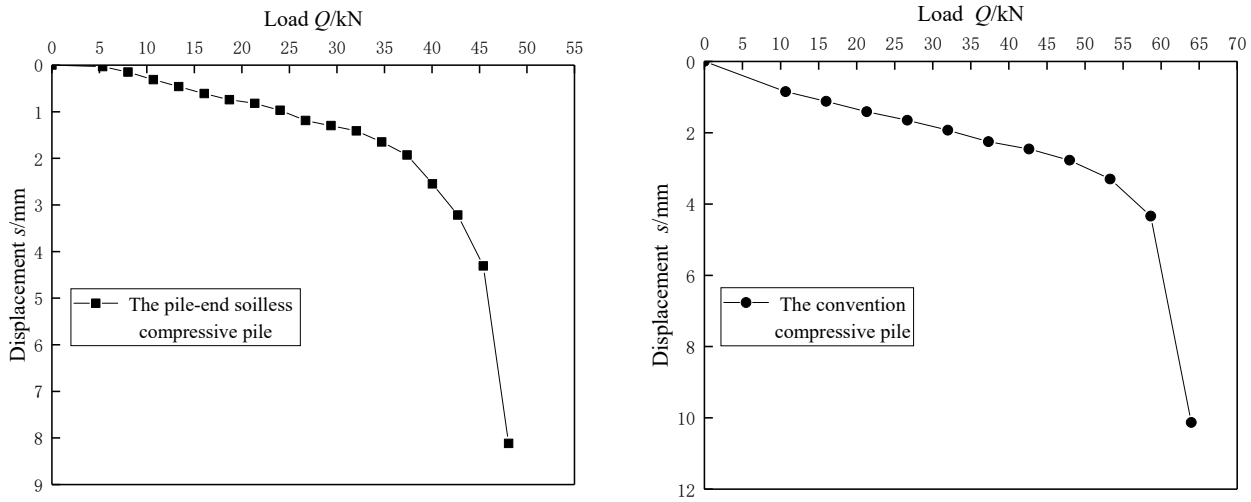

(**a**) (**b**)

Figure 4. Q-s curve of test pile: (**a**) the pile-end soilless compressive pile and (**b**) the conventional compressive pile.

From Figure 4a, it can be seen that the Q-s curve of the pile-end soilless compressive pile shows a slow–steep type. When the load is less than 13.35 kN, the pile-top settlement is small, and the settlement varies approximately linearly with the increase of the load. As the load increases, the Q-s curve gradually bends, and the settlement rate increases, showing a nonlinear change. When the load is greater than 40.05 kN, the settlement rate of the pile top increases rapidly, and the Q-s curve shows a steep drop point at 45.39 kN. The cumulative settlement of the pile top is 4.31 mm. Figure 4b show the Q-s curve of the conventional compressive pile, which is consistent with the trend of the curve of the pile-end soilless compressive pile, and the curve shows a slow–steep type. When the load is less than 21.32 kN, the pile top settlement is small. As the load increases, the Q-s curve

gradually bends, and the settlement rate of the pile top increases, showing a nonlinear change. When the load is greater than 53.3 kN, the settlement rate of the pile top increases rapidly, and the Q-s curve shows a steep drop point at 58.63 kN. The cumulative settlement of the pile top is 4.34 mm.

The overall performance of the Q-s curves of the two test piles is relatively consistent, and the Q-s curves can be divided into three stages: the linear stage, the local shear stage, and the failure stage. For the pile-end soilless compressive pile, when the load is in the range of 0–10.68 kN, the Q-s curve is approximately a straight line, showing that the pile body is in a linear stage. When the load is in the range of 13.35–40.05 kN, the Q-s curve changes nonlinearly, the pile top settlement increases significantly, and the soil around the pile gradually changes nonlinearly, showing that the pile body is in the local shear stage. When the load is in the range of 42.72–48.06 kN, the pile top settlement increases rapidly, and when the soil around the pile is damaged, the pile displacement will increase sharply, and the whole pile slides downward, at which time the pile is in the failure stage. Similarly, the conventional compressive pile is divided into three stages: When the load is 0–15.99 kN, it is the linear stage. When the load is 21.32–53.3 kN, it is the local shear stage. When the load is 58.63–63.96 kN, it is the failure stage. Different from the pile-end soilless compressive pile, when the conventional compressive pile is in the failure stage and the soil at the end of the pile is damaged by compression, the pile displacement will increase sharply, and the whole pile will slide downward.

Based on the measured data, the s-lgt curves of the two test piles under different static loads were obtained, as shown in Figure 5.

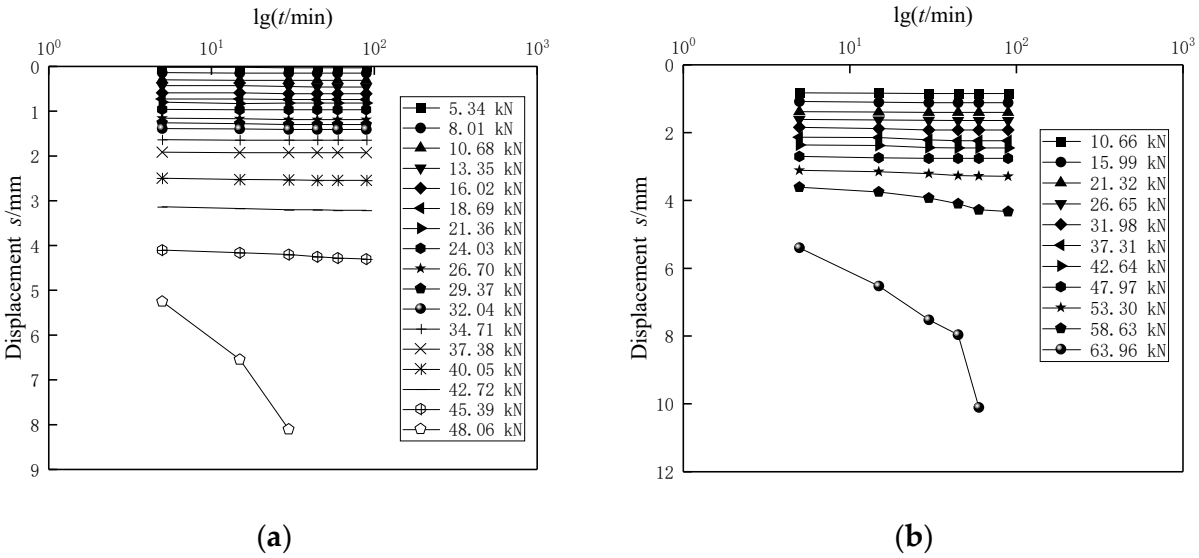

(**a**) (**b**)

Figure 5. s-lgt curves of test pile: (**a**) the pile-end soilless compressive pile and (**b**) the conventional compressive pile.

From Figure 5a, after the pile-end soilless compressive pile was loaded to 48.06 kN, the pile top settlement suddenly increased to 8.12 mm, and the soil around the pile was damaged. Combined with Figure 4a, 45.39 kN was the ultimate bearing capacity of the pile-end soilless compressive pile. From Figure 5b, after the conventional compressive pile was loaded to 63.96 kN, the pile top settlement suddenly increased to 10.13 mm, and the pile-end soil was damaged. Combined with Figure 4b, 58.63 kN was the ultimate bearing capacity of the conventional compressive pile.

Compared with the ultimate bearing capacity, the linear section of the pile-end soilless compressive pile accounts for about 23.5% before the ultimate bearing capacity, and the linear section of the conventional compressive pile accounts for about 36.4% before the ultimate bearing capacity. This shows that the length of the linear section on the Q-s

curve of the pile-end soilless compressive pile is smaller than that of the linear stage of the conventional compressive pile, and the conventional compressive pile has better ductility.

3.2. Analysis of Pile Axial Force

Through the strain gauges set on the pile body, the strain at each section of the pile body under different loads can be obtained, and the axial force of the pile at each section can be calculated. The calculation formula is:

$$P_i = A_p \cdot E_p \cdot \varepsilon_i. \quad (1)$$

Here, A_p represents the cross-sectional area of the pile. E_p represents the elastic modulus of the pile. ε_i is the strain at the pile section i. P_i represents the value of the axial force at the pile section i.

The variation curves of the pile axial force magnitude along the depth for the pile-end soilless compressive pile and the conventional compressive pile are shown in Figure 6.

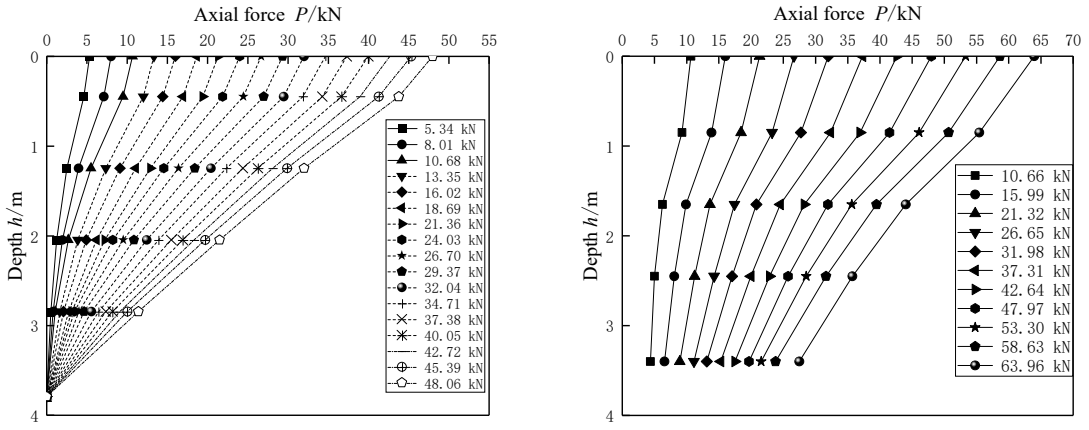

(**a**) (**b**)

Figure 6. Axial force distribution curve of test pile body: (**a**) the pile-end soilless compressive pile and (**b**) the conventional compressive pile.

Under the vertical load, the axial elastic compression of the pile causes the relative displacement of the pile and soil, thereby generating the skin friction, while the vertical load overcomes the skin friction and transmits down the pile body. As shown in Figure 5, the axial force curve of the pile body is roughly linearly distributed. The steepness of different segments reflects the size of the skin friction of the segment; the steeper the curve, the smaller the skin friction, and vice versa, the greater the skin friction. At the initial stage of loading, the slope change of the axial force curve on the upper part of both test piles is relatively obvious, which indicates that the skin friction at the pile body is fully exerted. At the same depth, as the load increases, the slope of the axial force distribution curve gradually decreases until it is stable. This shows that the skin friction develops gradually with the increase of the load and finally tends to be stable. This is mainly because when the load is gradually increased, the compression and displacement of the pile body increase and the skin friction increases with the increase of the relative displacement until it reaches stability.

Under different loads, the axial force of the two test piles gradually decreases downward with the depth, reflecting the characteristics of the skin friction gradually exerting from top to bottom along the pile body, and the axial force distribution forms are basically similar but also different: For the axial force distribution of the pile-end soilless compressive pile (Figure 6a), the axial force at the pile-end soilless compressive pile is zero during loading, which directly reflects the successful fabrication of the pile-end soilless compressive pile. The loads are balanced by the skin friction provided by the pile-side soil, and the

curves are uniformly distributed as the load increases. For the axial force distribution of conventional compressive pile (Figure 6b), the load is mostly borne by the skin friction during the initial loading period. With the increase of the load, the resistance of the pile-end is gradually exerted. Under the ultimate load, the slope of the axial force curve of the pile body becomes smaller, and the axial force at the end of the pile is about 42% of the pile top load, exhibiting the characteristics of an end-bearing friction pile.

3.3. Analysis of the Skin Friction

According to the difference between the axial force of the pile body between the two measuring points divided by the pile side surface area of the section, the skin friction f_i of the section can be obtained. The calculation formula is:

$$f_i = \frac{P_{i-1} - P_i}{U \cdot l_i} \quad (2)$$

where P_{i-1}, P_i represents the axial force values of two adjacent measurement points above and below the pile section i. U represents the pile circumference. l_i represents the length of the pile section i.

From the calculation results, the skin friction distribution curves of the two test piles are obtained. The linear stage is a solid line, the local shear stage is a dashed line, and the failure stage is a dotted line, as shown in Figure 7.

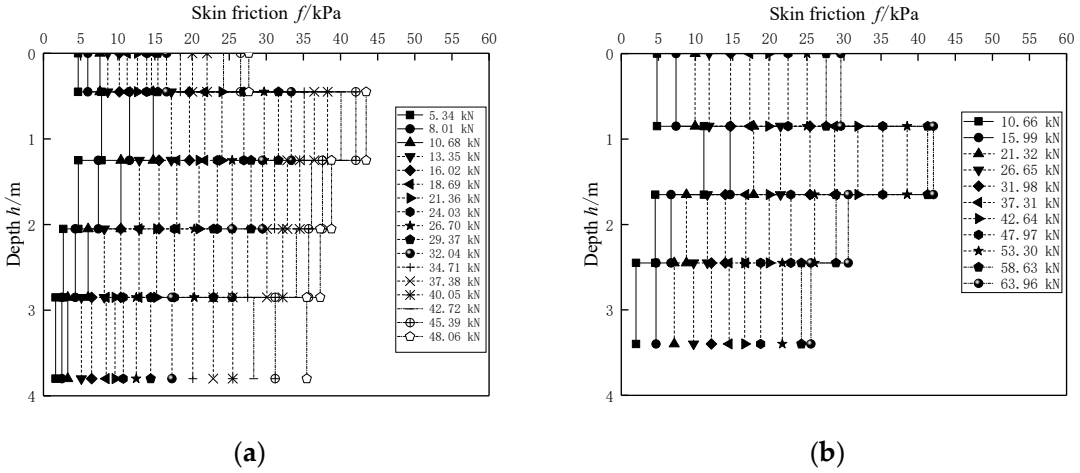

(**a**) (**b**)

Figure 7. Distribution curve of the skin friction: (**a**) the pile-end soilless compressive pile and (**b**) the conventional compressive pile.

In Figure 7, it can be seen that skin friction is gradually exerted with the increase of the load. Affected by the load, the pile body is compressed and deformed, resulting in the relative displacement of the pile and the soil around the pile, thus generating skin friction to bear the upper load. Overall, skin friction tends to increase first and then decrease and increase as the load increases, and the curve is characterized by "small on both sides and large in the middle". Both piles decrease skin friction along the pile body after peaking with increasing load, and the rate of decrease is greater for conventional piles than for pile-end soilless compressive pile. At the ultimate load, the maximum skin friction of the pile-end soilless compressive pile is 43.46 kPa, and the maximum skin friction of the conventional compressive pile is 42.06 kPa. The soil layers corresponding to the peaks of the skin friction of the two piles are silty clay–muddy silty clay layers. The maximum skin friction of the two piles is similar in value, indicating that the skin friction performance of the two test piles in this soil layer is almost the same. At the pile-end position, the skin friction of the two piles are 35.45 kPa and 25.55 kPa, respectively. The skin friction of the conventional compressive pile is about 28% lower than that of the pile-end soilless compressive pile.

3.4. Evolution of the Skin Friction

The skin friction distribution curve is normalized, and the abscissa is defined as the segment skin friction divided by the maximum skin friction of the test pile at this level of load, which becomes the pile segment skin friction ratio, and the ordinate is defined as the position of the strain gauge divided by the pile length to become the depth ratio. The normalized curve is shown in Figure 8. The pile-end soilless compressive pile are solid lines, and the conventional compressive pile are dashed lines. In order to describe the variation law of the skin friction ratio of the pile segment conveniently, define 0–0.25 L as the upper part of the pile, 0.25 L–0.5 L as the upper-middle part of the pile, 0.5 L–0.75 L as lower-middle part of the pile, and 0.75 L–L as the lower part of the pile; the length of the pile is L. Figure 8 correspond to the distribution changes and comparisons of the pile segment skin friction ratio of the two piles in the linear stage, the local shear stage, and the failure stage.

In Figure 8a, in the linear phase, the pile side frictional resistance of both piles increases and then decreases in the direction of the pile body, and the peak value occurs in the middle and upper part of the pile. In the upper area of the two piles, the pile segment skin friction ratio of the pile-end soilless compressive pile decreases from 0.6 to 0.51, while the pile segment skin friction ratio of the conventional compressive pile increases from 0.43 to 0.5. This indicates that the performance of load transfer on the upper part of the pile-end soilless compressive pile is better than that of the conventional compressive pile when the test piles are in the linear stage.

In Figure 8b, In the local shear stage, with the increase of load, the distribution trend of skin friction of the two test piles continued to increase first and then decrease, and the location of peak skin friction did not change. In the upper part of the two piles, the lateral friction ratio of the pile section pile segment skin friction ratio of the two test piles increased continuously but more concentrated as the load increased, indicating that the two test piles behaved in a more consistent manner as the load increased and the skin friction provided by the soil around the upper part of the pile increased gradually reaching the limit. In the middle-lower sections of the pile, the pile segment skin friction ratio of the pile-end soilless compressive pile increases from 0.48 to 0.84, while the pile segment skin friction ratio of the conventional compressive pile increases from 0.49 to 0.68. In the lower part of the pile, the pile segment skin friction ratio of the pile-end soilless compressive pile increases from 0.3 to 0.67, while the pile segment skin friction ratio of the conventional compressive pile increases from 0.4 to 0.56. Compared with the conventional compressive pile, the pile segment skin friction ratio of the pile-end soilless compressive pile is more variable. It shows that as the load increases, the friction performance of the soil layer around the lower-middle part and lower part of two piles of the pile-end soilless compressive pile is better than that of the conventional compression pile. That is to say, the skin friction of the lower-middle part and lower part of the pile-end soilless compressive pile is exerted to an increasing degree.

A large number of experimental studies have shown that only when the vertical load reaches a certain value does the pile-end resistance gradually come into play, and then the pile-end resistance may have an effect on the skin friction. Therefore, the variation of skin friction under ultimate load is an effective means to study the effect of the presence of the pile-end soil on the pile skin friction. From Figure 8c, when the load is in the failure stage, the skin friction of both piles increases to different degrees. From the upper part of the pile to the middle-lower part of the pile, the skin friction of the pile-end soilless compressive pile is smaller than that of the conventional compression pile. In the lower part of the pile, the pile segment skin friction ratio of the pile-end soilless compressive pile increases from 0.71 to 0.82, while the pile segment skin friction ratio of the conventional compressive pile increases from 0.59 to 0.61. This shows that as the load increases to the failure stage, the skin friction of each pile section and the pile segment skin friction ratio also increases, and the laws of the two piles are relatively consistent. However, from the values of the pile segment skin friction ratio, the conventional compression pile is much smaller than the

pile-end soilless compressive pile, and the skin friction of the conventional compression pile shows an obvious weakening phenomenon. Combined with the skin friction values of the corresponding pile sections, the skin friction is 30.59 kPa for the conventional compressive pile and 37.27 kPa for the pile-end soilless compressive pile in the middle-lower part of the pile. The skin friction of the conventional compressive pile is about 18% lower than that of the pile-end soilless compressive pile. In the lower part of the pile, the skin friction of the conventional compression pile is 25.55 kPa, and the pile-end soilless compressive pile is 35.45 kPa. The skin friction of the conventional compressive pile is about 28% lower than that of the pile-end soilless compressive pile. This weakening effect exists in the middle and lower parts of the pile, and the weakening effect decreases from bottom to top.

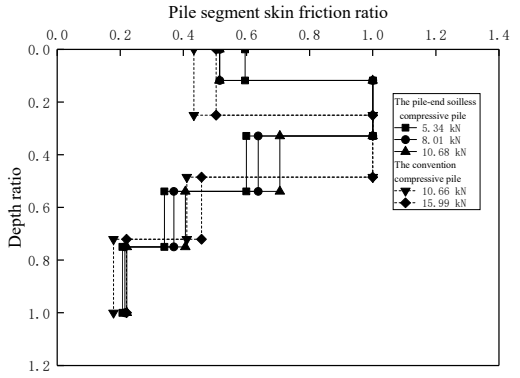

(**a**)

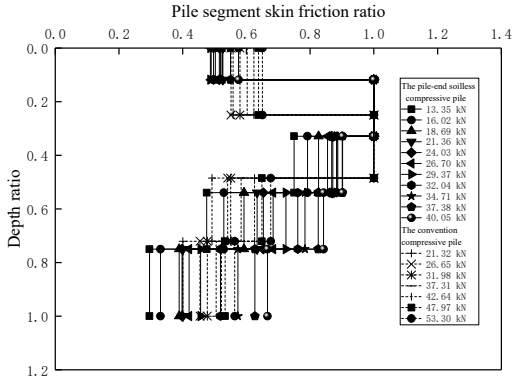

(**b**)

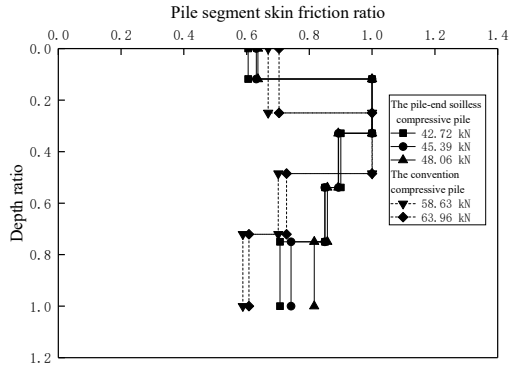

(**c**)

Figure 8. Distribution curve of the pile segment skin friction ratio along depth: (**a**) the linear stage, (**b**) the local shear stage, and (**c**) the failure stage.

In general, the skin friction of both piles is basically the same when subjected to vertical load, with the law of top-down gradual action. That is, the skin friction on the upper part of the pile bears the load first, and as the load continues to increase, the skin friction on the lower part of the pile comes into play. The distribution form and distribution pattern of the pile segment skin friction ratio is more consistent between the two piles, while the difference in the magnitude of the pile segment skin friction ratio reflects the difference between the two piles. For the pile-end soilless compressive pile, from the linear stage to the local shear stage to the final failure stage, the skin friction of each pile section reaches the limit, and then the soil around the pile breaks down, and the pile top load reaches the maximum. For the conventional compressive pile, from the linear stage to the local shear stage to the final failure stage, skin friction comes into play continuously, and the end resistance also comes into play gradually as the load increases. Different from the pile-end soilless compressive pile, the skin friction of some pile sections is not kept consistent. This may be due to the presence of the pile-end soil, which provides an end resistance that limits the skin friction, which shows a weakening effect.

4. Conclusions

Based on the in situ experiment, this paper compares and analyzes the difference in load transfer laws between the pile-end soilless compressive pile and the conventional compressive pile and draws the following conclusions:

1. The Q-s curves of both the pile-end soilless compressive pile and the conventional compressive pile have obvious inflection points and show a slow–steep drop type. The linear section of the pile-end soilless compressive pile accounts for about 23.5% before the ultimate bearing capacity, and the linear section of the conventional compressive pile accounts for about 36.4% before the ultimate bearing capacity. This shows that the conventional compressive pile has better ductility.
2. During the whole loading process, the peak position of the skin friction of the two types of piles is in the middle-upper part of the pile, and the surrounding soil layers are all silty clay–muddy silty clay layers, and the skin friction provided by the soil layers to the two piles is basically the same.
3. When the two piles are loaded, the skin friction is basically the same as the top-down gradual effect of the law, and the distribution form and distribution law of the pile segment skin friction ratio is more consistent between the two piles.
4. Compared with the pile-end soilless compressive pile, the pile-end soil of the conventional compressive pile restricts the skin friction of the middle-lower part of the pile and the lower pile section, and this restriction is manifested as a weakening effect on the skin friction of the pile, and the weakening effect is 18% and 28% in turn.

The research conclusion of this paper is based on the steel pile. Due to the great difference between the material of concrete pile and steel pile and the manufacturing method of the pile, the applicability of this conclusion to concrete pile needs further study.

Author Contributions: Conceptualization, H.M. and H.Z.; methodology, H.M. and H.Z.; software, H.Z.; validation, H.Z.; formal analysis, H.Z.; investigation, H.Z.; resources, H.M.; data curation, H.Z.; writing—original draft preparation, H.Z.; writing—review and editing, H.Z.; visualization, H.M.; supervision, H.M.; project administration, H.M.; funding acquisition, H.M. All authors have read and agreed to the published version of the manuscript.

Funding: This research was funded by the National Natural Science Foundation of China, grant number 51878618.

Institutional Review Board Statement: Not applicable.

Informed Consent Statement: Not applicable.

Data Availability Statement: All data generated or analysed during this study are included in this published article.

Conflicts of Interest: The authors declare no conflict of interest. The funders had no role in the design of the study; in the collection, analyses, or interpretation of data; in the writing of the manuscript, or in the decision to publish the results.

References

1. Ghasemzadeh, H.; Tarzaban, M.; Hajitaheriha, M.M. Numerical analysis of pile–soil–pile interaction in pile groups with batter piles. *Geotech. Geol. Eng.* **2018**, *36*, 2189–2215. [CrossRef]
2. Wu, Y.D.; Ren, Y.Z.; Liu, J.; Ma, L. Analysis of negative skin friction on a single pile based on the effective stress method and the finite element method. *Appl. Sci.* **2022**, *12*, 4125. [CrossRef]
3. Lee, J.X. Analytical model and back-analysis for pile-soil system behavior under axial loading. *Ocean Eng.* **2018**, *152*, 17–25. [CrossRef]
4. Lv, Y.R.; Ding, X.M.; Liu, H.L. Mechanical response of pile-soil interactions of X-section cast-in-place concrete piles to cross-sectional shape. *Rock Soil Mech.* **2015**, *36*, 357–364.
5. Zhang, C.F.; Zhao, M.H.; Zhou, S. A theoretical solution for pile-supported embankment with a conical pile-head. *Appl. Sci.* **2022**, *9*, 2658. [CrossRef]
6. Khorami, F.G.; Rasoolan, I. Soil-pile interaction analysis using multi-laminate elasto-plastic modelling. *Geotech. Geol. Eng.* **2017**, *35*, 1665–1683. [CrossRef]
7. Henryk, P. Experimental verification of integrity of low-pressure injection piles structure-pile internal capacity. *Stud. Geotech. Mech.* **2018**, *39*, 77–85.
8. Nie, R.S.; Leng, W.M.; Yang, Q.; Wei, W. Discussion on shear stress transfer between pile and soil. *Rock Soil Mech.* **2019**, *30*, 799–804.
9. Chen, B.C.; Luo, X.Y. Displacement-based simplified calculation for pile-soil interaction under reciprocating low-cycle pseudo-static loads. *J. Test. Evalr.* **2021**, *49*, 2609–2626. [CrossRef]
10. Li, L.; Li, J.P.; Sun, D.A.; Gong, W.B. Nonlinear load-settlement analysis of pile groups considering pile installation effects. *Rock Soil Mech.* **2019**, *40*, 668–677.
11. Wu, S.S.; Hu, X.L.; Gong, H.; Zhou, C.; Xu, C.; Wang, Q.; Ying, C.Y. Shear properties of pile-soil of three modes of bored piles in field tests. *Rock Soil Mech.* **2019**, *4*, 2838–2846.
12. Wu, X.X. Interaction between end resistance and side friction of pile and its engineering application value. *J. Southwest Jiaotong Univ.* **1997**, *32*, 81–86.
13. Xi, N.Z. A discussion on influence of soil strength underneath a pile on the pile shaft resistance. *Build. Sci.* **2000**, *16*, 51–54.
14. Xiao, H.B.; Zhang, C.S. Mutual reinforcement of pile end soil and pile side soil during load transfer. *J. Zhuzhou Inst. Technol.* **2006**, *20*, 75–79.
15. Zhang, J.X.; Wu, D.Y. Research on interaction between resistance at pile and lateral resistance of pile. *Rock Soil Mech.* **2008**, *2*, 541–544.
16. Meyerhof, G.G. The ultimate bearing capacity of foundations. *Geotechnology* **1951**, *2*, 301–302.
17. Zhang, Z.M.; Zhang, Q.Q. Influences of soil strength at pile end on friction of lateral surface of piles. *Chin. J. Geotech. Eng.* **2010**, *32*, 59–63.
18. Liu, K.; Zhao, C.F. Model tests on bored piles under vertical load on different pile-tip soils. *Chin. J. Geotech. Eng.* **2011**, *33*, 490–495.
19. Dong, J.R. Enhanced and weakened effect of skin friction of cast-in-situ piles. *Chin. J. Geotech. Eng.* **2009**, *31*, 658–662.
20. Xiong, Y.C. Research on strength characteristics of sediment and hardening and softening effect of skin friction. *Ind. Constr.* **2019**, *49*, 107–114.
21. Ju, X.D.; Feng, W.J.; Zou, Z.S.; Zhang, Y.J. Numerical analysis of abnormal effect of skin friction on bored pile. *Ind. Constr.* **2014**, *44*, 661–665.
22. *JGJ 106-2014*; Technical Code for Testing of Building Foundation Piles. China Architecture & Building Press: Beijing, China, 2014.